

# Density dependent speed-up of particle transport in channels

Karolis Misiunas\* and Ulrich F. Keyser†  
Cavendish Laboratory, University of Cambridge, UK  
(Dated: December 14, 2024)

Collective transport through channels shows surprising properties under one-dimensional confinement: particles in a single-file exhibit sub-diffusive behaviour, while liquid confinement causes distance-independent correlations between the particles. Such interactions in channels are well-studied for passive Brownian motion but driven transport remains largely unexplored. Here, we demonstrate gating of transport due to a speed-up effect for actively driven particle transport through microfluidic channels. We prove that particle velocity increases with particle density in the channel due to hydrodynamic interactions under electrophoretic and gravitational forces. Numerical models demonstrate that the observed speed-up of transport originates from a hydrodynamic piston-like effect. Our discovery is fundamentally important for understanding protein channels, transport through porous materials, and for designing novel sensors and filters.

On the nano- and micron-scale, electric fields acting on ionic charges provide the dominant driving force for transport in aqueous environments. The so-called electrophoresis of charged particles is important for many fields including filtration and separation technologies. In these systems, it is commonly assumed that electrophoretic motion is independent of particle-particle distance and hence density. Any long-range interactions are routinely neglected in the thin Debye layer limit [1] because electroosmotic and Stokes contributions to the flow cancel each other in the bulk. However, this symmetry can be broken by the presence of a solid boundary, leading to significant particle interactions. The most extreme confinement of particles is found in channel geometries approaching the single-file limit. Examples include protein channels in biology [2], nanopore sensors [3, 4], porous rocks, and filtration membranes [5]. In all these cases, channels accommodate the transport of charged ions, molecules, or particles. Particle interactions in channels have been extensively studied, especially in the free Brownian motion regime [6–9]. In microfluidic systems, particles experience long-range hydrodynamic interactions that are independent of inter-particle distances [9]. These interactions arise due to momentum transfer from the moving particle to the liquid and then from the liquid to other particles [10]. However, in the case of particle electrophoresis in channels, recent theoretical analyses found no long-range interactions [11, 12]. On the contrary, the studies predict that the inter-particle interactions only extend to distances similar to the channel width. The difference between experimental [9] and theoretical studies [11, 12] raises fundamental questions on the relevance of interactions for driven particle transport.

One striking example of the profound effects of particle-particle interactions on single-file transport is the stochastic gating observed in highly selective ion channels [13]. Such systems with diameters of a few angstroms

allow the passage of ions via the multi-ion ‘knock-on’ mechanism [14]. The stochastic transport leads to abrupt variations in the observed ionic currents in the time domain, known as gating [13], often associated only with nanoscale systems. In this paper, we show that distance-independent hydrodynamic interactions present in microfluidic channels [9] gives rise to stochastic behaviour akin to gating in biological ion channels.

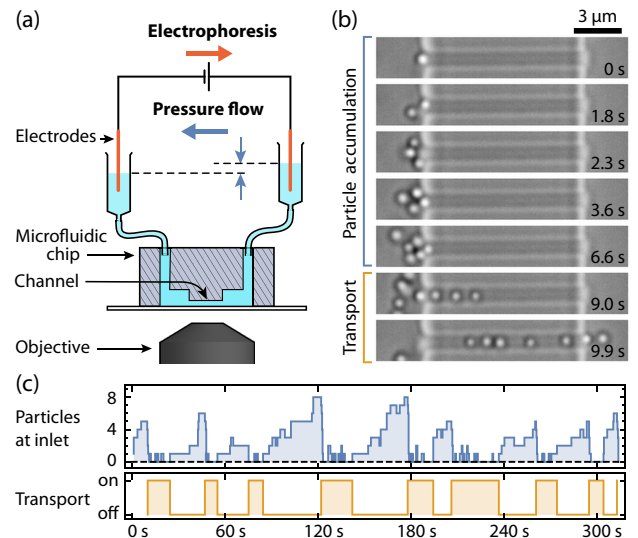


FIG. 1. (a) Schematic of experimental setup that allows for simultaneous control of the electric field and the pressure across the channel. (b) Micrographs show particle accumulation at the channel inlet with no transport because pressure flow dominates. However, at high particle densities, the particle-particle interactions dominate, thus allowing electrophoretic transport. (c) Number of particles at the channel inlet (blue) and transport (orange) shown as a function of time. Transport exhibits gating like behaviour between ‘on’ and ‘off’.

In our experiments, we investigate the influence of interactions between driven particles inside microfluidic channels. Our setup allows us to directly quantify the role of particle-particle interactions during electrophoresis in single-file channels. We simultaneously control

\* correspondence: karolis@misiunas.com

† correspondence: ufk20@cam.ac.uk

electric fields and pressure-driven flows, while also permitting direct imaging of particle motion. Figure 1a shows an illustration of our setup. Inside the microfluidic chip, two reservoirs are connected by narrow channels of length  $L = 10.0 \pm 0.5 \mu\text{m}$  and rectangular cross-section  $750 \pm 50 \text{ nm} \times 750 \pm 50 \text{ nm}$ . The chips are fabricated via replica moulding of polydimethylsiloxane (PDMS), where the master is made using e-beam lithography and photo-lithography; more details are published elsewhere [15, 30]. A PDMS copy is air plasma bonded to a glass slide that is coated with a sub  $100 \mu\text{m}$  PDMS layer, ensuring that all channel walls are made out of the same material [16].

An assembled chip is filled with KCl solution containing spherical polystyrene particles of diameter  $2a = 505 \pm 8 \text{ nm}$  (Polysciences Inc.). Their motion is imaged through an inverted optical microscope with a high numerical aperture oil immersion objective ( $100\times$ ; NA 1.4; UPLSAPO) and recorded using a camera (Mikrotron MC1362) at a rate of 200 frames per second. Afterwards, the particle trajectories are extracted using established image analysis techniques [17].

Particles are actively driven by an external electric field or/and a pressure flow. The electric field is applied using two Ag/AgCl-electrodes submerged in the external reservoirs. Electric potentials up to 1 V are applied using a digital to analogue converter (NI-USB-6211) controlled by a computer. The pressure flow is controlled by adjusting the relative height of the external reservoirs. After assembling the chip, we find the pressure equilibrium by adjusting the pressure until particles stop migrating to either end of the channel.

Balancing pressure and electrophoretic forces in our microfluidic channels gives rise to a regime that resembles stochastic gating found in biological channels. Figure 1b shows two distinct states that we define as particle accumulation and transport. During the accumulation, particles are electrophoretically pulled towards the channel, but the opposing pressure flow inside the channel prevents transport across. As a result, the particle number increases over time at the left inlet [18, 19]. Eventually, the transport starts when two or more particles randomly enter the channel. In this case, electrophoresis transiently dominates over the pressure and allows for transport. The transport ends when the last particle exits the channel.

Figure 1c shows the channel switching between the accumulation and the transport states. The blue line indicates that particles need to accumulate at the inlet, and that transport is possible only after 2 or more particles are present. The resulting transport (orange lines) resembles stochastic gating found in biological ion channels. Importantly, in our system the channel's conformation is fixed and gating is a consequence of competition between different physical forces. In order to elucidate the origin of the gating effect we performed experiments investigating both pressure and electrophoretically driven

transport separately.

We start by measuring the velocity of 1, 2 and 3 particles in a channel driven only by electric fields, as shown in Figure 2a. At  $t = 0$  the leftmost particles are aligned to the red line. After 800 ms the snapshot shows that the two particles travelled further than one particle; and three made it further than two, illustrating the unexpected increase in velocity with particle number.

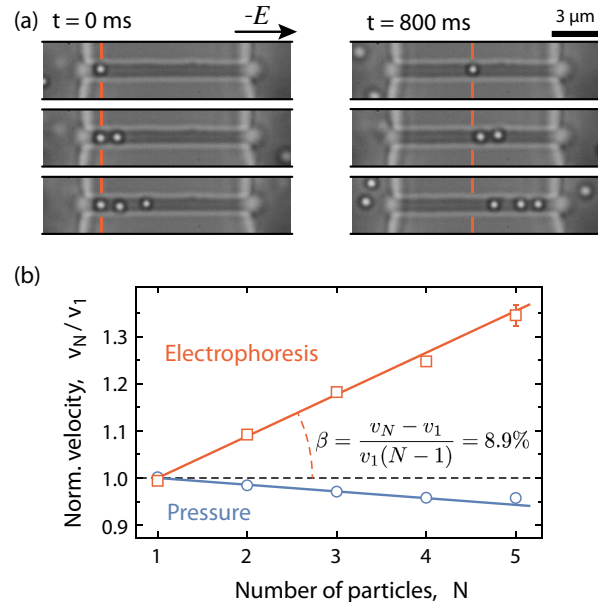


FIG. 2. Particle speed-up during electrophoresis. (a) The left column shows micrographs with one, two, and three particles in the channel with leftmost particles aligned to the red line. The negatively charged particles migrate in an electric field for 800 ms and the resulting micrographs are shown on the right column. Red lines guide the eye. Three particles traveled further than 2 and 1 after 800 ms. (b) Normalised particle velocity ( $v_N/v_1$ ) as a function of particle number  $N$  for electrophoretic transport (red) and for pressure-driven transport (blue). Errors are smaller than the marker sizes, except for  $N = 5$ . Lines are weighted linear fits. The velocity linearly increases with  $N$  under electrophoresis but reduces under pressure flow.

Quantitatively, we analyse the particle trajectories by measuring the velocity as a function of particle number,  $N$ , inside the channel. Only particles separated by more than  $1.2 \mu\text{m}$  are analysed, thus excluding any close range effects [9, 11]. In addition, we disregard all parts of the trajectories within  $0.5 \mu\text{m}$  of the channel ends to ensure diffusion coefficients are constant [20]. The remaining trajectory segments are averaged while retaining the particle count.

The red points in Figure 2b show normalised velocity ( $v_N/v_1$ ) as a function of  $N$  for electrophoretic motion, while keeping the pressure flow at zero (estimated from  $\sim 38000$  video frames of more than 650 particles). The normalisation velocity is  $v_1 = 17.48 \pm 0.08 \mu\text{m/s}$  at an applied potential of 200 mV. The velocity linearly increases with  $N$ , clearly contradicting the previous theo-

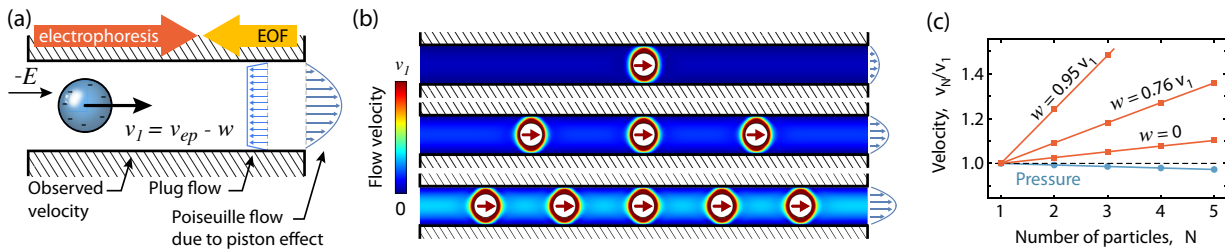


FIG. 3. Simulation results. (a) The applied external field,  $E$ , drives a negatively charged particle through a finite channel at velocity  $v_{ep}$ , giving rise to a Poiseuille flow due to a piston effect. Simultaneously, negatively charged walls induce an electro-osmotic plug flow (EOF) in the opposite direction at velocity  $w$ . (b) Simulated flow velocities for one, three, and five particles driven through a channel by an electric field (red arrow indicates the direction of force) for  $w = 0$ . The Poiseuille flow increases with particle number in the channel. (c) The predicted normalised particle velocity,  $v_N/v_1$ , increases with  $N$  for particles driven by electric field (red), but decreases for pressure driven particles (blue).

retical predictions [11, 12].

After driving the particles by electric fields we now investigate the velocity under pressure driven flows. The blue data in Figure 2b shows the results performed in the same microfluidic systems with particles from the same batch. The normalisation velocity is  $v_1 = 68.10 \pm 0.06 \mu\text{m/s}$  at height difference of 11.9 mm that produces the pressure flow. The velocity decreases slightly with the number of particles in contrast to the electrophoresis results.

The stark difference between the particle interactions, allows us to explain the observed gating behaviour in Figure 1b. The pressure-driven velocity stays roughly constant for all  $N$  and blocks transport for  $N = 1$ . However, for  $N \geq 2$ , electrophoretic velocity increases due to the speed-up (Figure 2b) and overcomes the opposing pressure flow. Thus when more than two particles enter the channel, electrophoresis transport is permitted, until  $N = 0$  and accumulation starts again.

Having explained the observed gating, we now quantify the underlying phenomena. To compare the different driving forces we define an *interaction coefficient*:  $\beta \equiv \Delta v/v_1$ , where  $\Delta v = v_{N+1} - v_N$  is the averaged speed-up due to each additional particle.  $\beta$  can be extracted from the slope of the curves in Figure 2b. For electrophoresis,  $\beta = 8.9 \pm 0.2\%$  at 2 mM KCl and pH 7.2. Meanwhile, for the pressure driven transport  $\beta = -1.43 \pm 0.07\%$ . The interaction coefficient corresponds to the fraction of velocity gained with each additional particle inside the channel.

As we are unaware of any analytical solutions for electrokinetic transport, we model the particle velocity using a numerical model implemented using COMSOL Multiphysics (v4.4). Our model is accessible online [21]. Before we discuss the details of the model we introduce the relevant electrokinetic effects in Figure 3a. We use an axial-symmetric channel containing a spherical particle in a uniform electric field ( $E$ ), as shown in Figure 3a. The particle carries a negative surface charge, while the charge on the channel walls has the same sign but varied magnitude. We assume a low Reynolds num-

ber regime and that flows have no-slip boundary conditions at the walls. The electrophoretic force drives the particle through the channel at a velocity  $v_{ep}$  resulting in the liquid being pushed forwards, resembling a piston effect. The resulting Poiseuille flow is indicated on the right of Figure 3a. In the case where the channel walls carry a negative charge, the well-known electro-osmotic plug flow (EOF) develops with velocity  $w$  moving in the opposite direction to  $v_{ep}$  [22].

In contrast to the literature [11, 12], we adopt open boundary conditions[23] at the inlets to account for the finite channels, which allow for critically important flows, thus enabling hydrodynamic interactions [9].

Figure 3b summarises the key results of our simulations with color maps depicting fluid flows for  $N = 1, 3$ , and 5. The first row of Figure 3b shows the flow velocity for  $N=1$  due to electrophoretic body force (indicated by the red arrow in the particle). The particle's motion induces a finite Poiseuille flow as illustrated by the profile on the right. Increasing  $N$  to 3 and 5 in rows two and three, respectively, increases the magnitude of the Poiseuille flow. The enhanced net flow throughout the channel is easily observed by the change in color from dark to light blue. Importantly, increased Poiseuille flows increase the velocity of all particles.

Figure 3c shows quantitative predictions of our simulations for particles driven by electrophoresis (red) and pressure driven flows (blue). The simulation parameters were selected to match our experiments with  $2a = 500 \text{ nm}$ ;  $L = 10 \mu\text{m}$ ; and  $2R = 840 \text{ nm}$ , where this diameter corresponds to the channel's cross-section area in the experiments [24, 30]. The first observation is that the slope of  $v_N/v_1$  clearly depends on the type of driving force; similar to the experiments. For particles driven by electrophoresis  $v_N/v_1$  linearly increases with  $N$  (red lines). The corresponding  $\beta = 2.6\%$  for simulation with no EOF ( $w = 0$ ). In contrast, particles carried by a pressure flow exhibit a decreasing  $v_N/v_1$  with  $N$  (blue curve) and a negative  $\beta = -0.69\%$ . This decreasing velocity is due to particles perturbing the optimal flow profile, thus slowing down the pressure induced flow that carries

them [25].

The simulations also reveal that  $\beta$  depends on  $w$ . Figure 3c shows simulations for three different surface charge densities that correspond to  $w/v_{ep} = 0.0, 0.76, \text{ and } 0.95$ . The resulting  $\beta$  coefficients are 2.6%, 8.9%, and 24.1%, showing that EOF velocity increases  $\beta$ .

The dependence of  $\beta$  on  $w$  can be explained by considering a linear superposition of the flows induced by electrophoresis and EOF. For one particle,  $v_1 = v_{ep} - w$ , as illustrated in Figure 3a. For  $N > 1$ , we can approximate  $v_N \approx v_{ep,N} - w$ , where  $v_{ep,N}$  indicates the electrophoretic velocity for  $N$  particles without the EOF and the approximation comes from non-linear components that are small and neglected for our salt concentrations [26]. As a result, the EOF contributions cancel, making  $\Delta v$  independent of the magnitude of EOF and thus  $\beta \approx \Delta v / (v_{ep} - w)$ . The  $\beta$  is a hyperbolic function with respect to  $w$  and  $v_1$ . We can maximise  $\beta$  with electrophoretic velocity matched by the EOF velocity and can minimize the interaction coefficient when  $w = 0$  (or negative). One important conclusion is that  $\beta$  is controlled by the channel surface charge and hence the EOF.

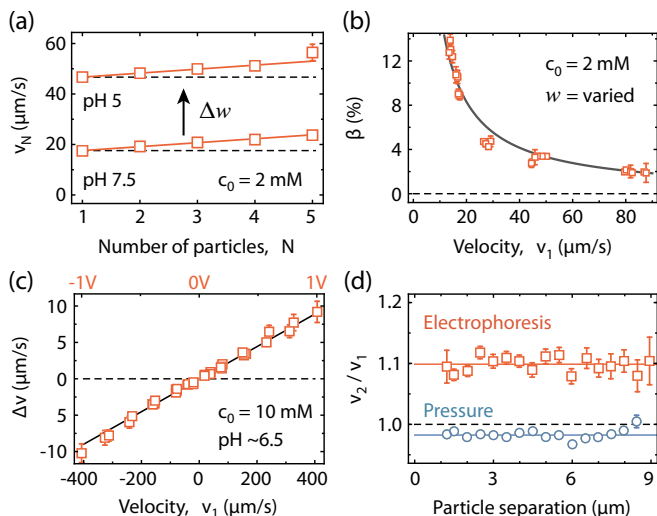


FIG. 4. (a) Velocity as a function of  $N$  for pH 5 and pH 7.5, which changes the surface charge density on the walls, thereby changing  $w$ . (b) Interaction coefficient,  $\beta$ , is shown as a function of particle velocity  $v_1$ . (c) Speed-up velocity,  $\Delta v$ , as a function of  $v_1$  and the applied voltage (top axis). (d) Normalised two particle velocity,  $v_2/v_1$ , is independent of the inter-particle distance.

In experiments, we are able to explore the relationship between  $\beta$  and  $w$  by adjusting the EOF. Figure 4a shows two measurements at pH 5 and pH 7.5 as a function of  $N$ . Decreasing pH decreases surface charge on the PDMS [22] and thus reduces  $w$ .  $v_1$  increases from  $17.5 \pm 0.1 \mu\text{m s}^{-1}$  to  $46.7 \pm 0.1 \mu\text{m s}^{-1}$ , while  $\Delta v$  stays roughly the same at  $\Delta v = 1.56 \pm 0.07 \mu\text{m s}^{-1}$  and  $\Delta v = 1.58 \pm 0.06 \mu\text{m s}^{-1}$ . As a result, the interaction coefficient decreases from  $\beta = 8.8 \pm 0.3\%$  to  $\beta = 3.4 \pm 0.2\%$ , proving the relationship with  $w$ .

Figure 4b shows  $\beta$  as a function of  $v_1$  for a wide range of  $w$  values.  $w$  was changed by varying the pH in the range from 5 to 10, and by exposing the channels to water for 1 hour, 12 hours, or 24 hours, which reduces the surface charge on the PDMS [27]. The measurements follow a hyperbolic curve, as expected. A weighted fit (grey line) to  $\beta = \Delta v / v_1$  gives  $\Delta v = 1.59 \mu\text{m s}^{-1}$ . The rightmost data points in Figure 4b have the smallest  $w$  that correspond to  $\beta = 1.80 \pm 0.14\%$ . This value is close to the simulation prediction for  $w = 0$ . Since we do not measure  $w$  directly in our experiment, it is the only fitting parameter in our model. The simulations agree very well with the experimental data, suggesting that our model captures the important physics.

Figure 4c shows the speed-up as a function of applied potential.  $\Delta v$  linearly increases with the applied electric potential (and  $v_1$ ), while  $\beta$  stays constant at 2.3%.  $\Delta v$  and hence the interaction strength scales linearly with the driving potential, thus affirming our choice the relative quantity  $-\beta$ .

In addition, we provide further evidence that the particle speed-up is indeed due to distance-independent hydrodynamic interactions. Figure 4d shows normalised two particle velocity,  $v_2/v_1$ , as a function of their separation distance. Evidently,  $v_2/v_1$  is independent of the separation distance for electrophoresis. We see the same characteristic in our hydrodynamics simulations (Figure S1) and similar distance-independent interactions were observed before but between freely diffusing particles in channels [9]. Combining all the experimental evidence with the simulations, suggests that the increase of particle velocity with  $N$  is caused by distance-independent hydrodynamic interactions.

Finally, we show that  $v_N$  increases for other body forces by changing the driving force to gravity. Gravity experiments are performed in the same microfluidic channels, but with gold particles of diameter  $2a = 400 \pm 50 \text{ nm}$  (supplied by CytoDiagnostics Inc.; in 0.1 mM PBS and 1 mM KCl). Gold particles have much higher mass density than water and thus the gravitational force is larger than for the polystyrene system used before. An assembled chip is mounted on a custom built rotatable microscope, as shown in Figure 5 inset. In contrast to the experiments using the pressure or the electric fields, gravity pulls the particles directly downwards without focusing them into the channels. This reduces the number of particles entering the channels and thus increases the uncertainty in our measurements ( $\sim 313000$  frames recorded at 30 fps of more than 330 particles). In addition, the net force on the particles reaches only about 6 fN (corresponding to  $v_1 = 0.23 \pm 0.02 \mu\text{m/s}$ ). Compared to thermal energy of  $\sim 4 \text{ pN nm}$ , fluctuation due to Brownian motion are significant and further increase variability.

Despite the experimental challenges, Figure 5 shows that gravity also exhibits the speed-up effect. A weighted fit gives an interaction coefficient of  $\beta = 18.9 \pm 3.4\%$ ,

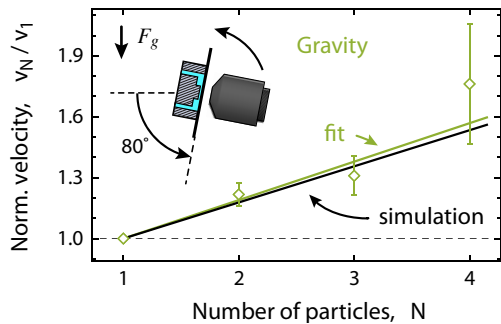


FIG. 5. Normalised particle velocity as a function of the particle number inside a channel for gravity propelled particles (green) compared to simulation results (black). Inset illustrates the setup for gravity experiments.

which agrees well with the corresponding simulation value of 17.9%. The simulation parameters were set to experimental values  $2a = 400$  nm;  $2R = 840$  nm and had no fitting parameters [30]. Our experiment confirms that the speed-up effect is universal for actively driven particles that are propelled by a body force.

The speed-up effect has important implications for understanding natural phenomena. We have demonstrated that it can cause gating like behaviour without conformational changes of the channel. This raises fundamental questions on how protein channels operate. In addition, the presence of constructive interactions suggests that particle transport rate through channels is a super-linear function of particle density. As a result, membranes with embedded channels should permit faster transport at higher particle densities. This can explain some of the peak tailing observed in electrochromatography or chromatography centrifuges because collectively particles travel faster than the isolated particles [28].

Although we only explored single-file transport, the speed-up is not limited to tightly confined particles and should persist for larger channels ( $a/R < 0.3$ ). In a large channel, each particle's piston-like contribution is small but the collective action of many particles should result in a net speed-up. Thus the speed-up effect might affect a wide range of confined systems, including self-propelled particles in confinement [29].

The phenomenon also enables novel technological applications. In particular, the particle accumulation at the inlet can be utilised to control a chemical reaction rate for manufacturing dimer particles. Or it could be used for particle separation. However, further investigations are necessary to fully realise all the technological opportunities presented by our discovery.

In conclusion, we have shown that particle transport velocity through channels increases with the particle number. We experimentally demonstrated that this happens with electrophoretically and gravity propelled particles but does not happen for pressure propelled particles. Our models suggest that the interactions are carried by hydrodynamics, where a piston-like motion of particles

induces a flow throughout the entire channel. These findings have far-reaching implications for transport through protein channels and enable novel technological applications.

We are grateful to Soichiro Tottori, Stefano Pagliara, Eric Lauga, Nicholas A.W. Bell, Vahe Tshitoyan, Jehangir Cama, and Alexander Ohmann for useful discussions. K.M. and U.F.K. acknowledge funding from an ERC consolidator grant (Designerpores 647144).

- 
- [1] Reed, L. D. & Morrison, F. A. Hydrodynamic interactions in electrophoresis. *Journal of Colloid And Interface Science* **54**, 117–133 (1976).
  - [2] Truskey, G. A., Yuan, F. & Katz, D. F. *Transport phenomena in biological systems* (Pearson Prentice Hall, 2009).
  - [3] Clarke, J. *et al.* Continuous base identification for single-molecule nanopore DNA sequencing. *Nature Nanotechnology* **4**, 265–270 (2009).
  - [4] Bell, N. A. W. & Keyser, U. F. Digitally encoded DNA nanostructures for multiplexed, single-molecule protein sensing with nanopores. *Nature Nanotechnology* **11**, 645–651 (2016).
  - [5] Ingham, D. B. & Pop, I. *Transport phenomena in porous media* (Elsevier Science, 1998).
  - [6] Diamant, H. Hydrodynamic interaction in confined geometries. *Journal of the Physical Society of Japan* **78**, 041002 (2009).
  - [7] Wei, Q.-H., Bechinger, C. & Leiderer, P. Single-file diffusion of colloids in one-dimensional channels. *Science* **287**, 625–627 (2000).
  - [8] Cui, B., Diamant, H. & Lin, B. Screened hydrodynamic interaction in a narrow channel. *Physical Review Letters* **89**, 188302 (2002).
  - [9] Misiunas, K., Pagliara, S., Lauga, E., Lister, J. R. & Keyser, U. F. Nondecaying hydrodynamic interactions along narrow channels. *Physical Review Letters* **115**, 038301 (2015).
  - [10] Lauga, E. & Powers, T. R. The hydrodynamics of swimming microorganisms. *Reports on Progress in Physics* **72** (2009).
  - [11] Hsu, J. P., Ku, M.-h. & Kao, C.-y. Electrophoresis of two identical cylindrical particles along the axis of a cylindrical pore. *Industrial & Engineering Chemistry Research* **44**, 1105–1111 (2005).
  - [12] Hsu, J. P. & Yeh, L. H. Electrophoresis of two identical rigid spheres in a charged cylindrical pore. *Journal of Physical Chemistry B* **111**, 2579–2586 (2007).
  - [13] Roux, B. *Ion channels and ion selectivity* (Sinauer, 2017).
  - [14] Roux, B. Ion channels and ion selectivity Essays in Biochemistry Benoit. *Essays in Biochemistry* **61**, 201–209 (2017).
  - [15] Pagliara, S., Chimere, C., Langford, R., Aarts, D. G. a. L. & Keyser, U. F. Parallel sub-micrometre channels with different dimensions for laser scattering detection. *Lab on a Chip* **11**, 3365 (2011).
  - [16] Deshpande, S., Caspi, Y., Meijering, A. E. C. & Dekker, C. Octanol-assisted liposome assembly on chip. *Nature Communications* **7**, 10447 (2016).
  - [17] Dettmer, S. L., Keyser, U. F. & Pagliara, S. Local charac-

- terization of hindered Brownian motion by using digital video microscopy and 3D particle tracking. *Review of Scientific Instruments* **85**, 023708 (2014).
- [18] Rempfer, G. *et al.* Selective Trapping of DNA Using Glass Microcapillaries. *Langmuir* **32**, 8525–8532 (2016).
- [19] Hoogerheide, D. P., Lu, B. & Golovchenko, J. A. Pressure-voltage trap for DNA near a solid-state nanopore. *ACS Nano* **8**, 7384–7391 (2014).
- [20] Dettmer, S. L., Pagliara, S., Misiunas, K. & Keyser, U. F. Anisotropic diffusion of spherical particles in closely confining microchannels. *Physical Review E* **89**, 062305 (2014).
- [21] COMSOL simulation code.  
URL [github.com/kmisiunas/speed-up-simulation](https://github.com/kmisiunas/speed-up-simulation).
- [22] Kirby, B. J. & Hasselbrink, E. F. Zeta potential of microfluidic substrates: 2. Data for polymers. *Electrophoresis* **25**, 203–13 (2004).
- [23] Alternatively, the periodic boundary conditions can be used with equivalent results. See the Supplementary Information for details.
- [24] Pagliara, S. *et al.* Diffusion coefficients and particle transport in synthetic membrane channels. *The European Physical Journal Special Topics* **223**, 3145–3163 (2014).
- [25] Happel, J. & Brenner, H. *Low Reynolds number hydrodynamics* (Springer, 1981).
- [26] Liu, Y.-w., Pennathur, S. & Meinhart, C. D. Electrophoretic mobility of a spherical nanoparticle in a nanochannel. *Physics of Fluids* **26**, 112002 (2014).
- [27] Bodas, D. & Khan-Malek, C. Hydrophilization and hydrophobic recovery of PDMS by oxygen plasma and chemical treatment An SEM investigation. *Sensors and Actuators B: Chemical* **123**, 368–373 (2007).
- [28] Sun, Y., Kwok, Y. C. & Nguyen, N. T. Modeling and experimental characterization of peak tailing in DNA gel electrophoresis. *Microfluidics and Nanofluidics* **3**, 323–332 (2007).
- [29] Wioland, H., Lushi, E. & Goldstein, R. E. Directed collective motion of bacteria under channel confinement. *New Journal of Physics* **18** (2016).
- [30] See Supplemental Material [url], which includes Ref. [31].
- [31] Papanastasiou, T. C., Malamataris, N. & Ellwood, K. A new outflow boundary condition. *International Journal for Numerical Methods in Fluids* **14**, 587–608 (1992).